JOURNAL OF SOLID STATE CHEMISTRY 56, 171–181 (1985)

X-Ray Analysis of the Structural and Dynamic Properties of $BaFe_{12}O_{19}$ Hexagonal Ferrite at Room Temperature

X. OBRADORS,* A. COLLOMB, AND M. PERNET

Laboratoire de Cristallographie, Centre National de la Recherche Scientifique, Laboratoire associé à l'USMG, 166X, 38042 Grenoble Cédex, France

D. SAMARAS

Laboratoire de Science des Métaux, Faculté Polytechnique, Université Aristote, Thessalonique, Greece

AND J. C. JOUBERT

Laboratoire de Génie Physique, INPG, 38040 Grenoble, France

Received July 18, 1983; in revised form March 22, 1984

The room temperature crystal structure of $BaFe_{12}O_{19}$ hexagonal ferrite has been refined from X-ray single crystal data. This compound is hexagonal, space group $P6_3/mmc$, with two formula units per cell and cell parameters $a = 5.8920(1)$ Å and $c = 23.183(1)$ Å. The crystal structure has been refined to a final R value of 1.6% for 380 independent reflections. Three different models are considered for the structural and dynamic characteristics of the bipyramidal Fe ions: (1) a nondisordered configuration, (2) a static disorder between two adjacent pseudotetrahedral sites, and (3) a dynamical disorder between these sites. The X-ray results show that the bipyramidal Fe ions have a disordered configuration and previous Mössbauer spectroscopy studies prove that, at room temperature, the disorder is a dynamical one. The observed oxygen thermal relaxation, Fourier-difference peaks, and interatomic distances are consistent with a fast diffusional motion of the bipyramidal Fe ions within a quasiharmonic double-well potential.

Introduction

Hexagonal ferrites are a large family of hexagonal or rhombohedral ferrimagnetic oxides with interesting applications as permanent magnets or microwaves devices materials. Their crystal structures can be described by the superposition of some fundamental structural blocks formed by a close packing of hexagonal or cubic-stacked layers with composition BaO_3 and O_4. In this framework the metallic ions are located in octahedral and tetrahedral interstices.

The best known of these structures is the hexagonal M structure of $BaFe_{12}O_{19}$, isotype to the mineral magnetoplumbite (*1*) which can be described symbolically as

* Now at Dept. Física Atómica y Nuclear, Facultad de Física, Universidad de Barcelona, Diagonal 645, Barcelona-28, Spain. Author to whom all correspondence should be addressed.

0022-4596/85 $3.00

RSR*S* where R is a three-oxygen layer block with composition $(Ba^{2+}Fe_6^{3+}O_{11})^{2-}$ and S is a two-oxygen layer block with composition $(Fe_6^{3+}O_8)^{2+}$. The * symbol refers to the fact that the block preceding it has been turned 180° around the hexagonal c axis by a 6_3 symmetry axis (*2*). In this crystal structure the iron atoms are distributed within three different kinds of octahedral sites, one tetrahedral site and one trigonal bipyramid site. The hexagonal unit cell of dimensions $a \simeq 5.89$ Å and $c \simeq 23.2$ Å contains two formulae and is made up of 10 oxygen layers.

The crystal structure of $BaFe_{12}O_{19}$ (space group $P6_3/mmc$) was studied for the first time by Townes *et al.* in 1967 (*3*). In this work, the fundamental structural characteristics of the magnetoplumbite structure were determined. Nevertheless, some ambiguities remain about the actual structure and dynamic properties of the Fe atoms in the bipyramidal atomic sites. Townes suggested that these cations could be displaced from the 2*d* position, in the BaO_3 mirror plane (model 1), into the 4*e* positions, 0.156 Å away from the mirror plane, with half occupation (model 2) (Fig. 1). However, no conclusion was given about the nature of the disorder.

Actually, two possibilities arise for model 2: (a) a statical disorder of two Fe cations within the four tetrahedral equivalent 4*e* positions (model 2a), or (b) a dynamical disorder with a fast hopping of these cations through the 2*d* triangular position (model 2b).

The dynamical properties of Fe-bipyramidal atoms and their temperature dependence have been extensively studied by several authors using Mössbauer spectroscopy (*4–6*). Rensen and van Wieringen (*4*) and Mamalui *et al.* (*5*) have shown that, above $T \simeq 80$ K, the bipyramidal ^{57}Fe Lamb–Mössbauer factor is strongly anisotropic, being much smaller in the [001] direction. Below this temperature, the anisotropy of the f-factor decreases. Kreber *et al.* (*6*) have reported the existence of a discontinuity of the electric quadrupole hyperfine interaction at about the same temperature. The authors interpreted these experimental observations by means of a simple model in which the bipyramidal Fe atom jumps, at high temperature, from one pseudotetrahedral site to the opposite one, and below $T \simeq 80$ K freezes in one of these positions.

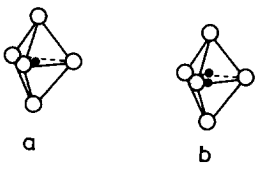

FIG. 1. Trigonal bipyramid sublattice: (a) model 1 and (b) model 2.

A knowledge of the precise structural characteristics of the bipyramidal cations is very important for the theoretical understanding of $BaFe_{12}O_{19}$ magnetic anisotropy (*7–9*). Therefore, we have undertaken a full study of its structural and dynamic properties at low and high temperature. This paper describes an accurate $BaFe_{12}O_{19}$ crystal structure refinement at room temperature, based on single crystal X-ray diffraction data and concentrates on three different models for the structural and dynamic properties of the bipyramidal Fe cation.

Experimental

Single crystals of $BaFe_{12}O_{19}$ were grown from a flux melt of composition $NaFeO_2$ + $BaFe_{12}O_{19}$ as stated by Gambino and Leonhard (*10*). A platinum crucible containing the components was placed in a programmable temperature furnace at 1573 K during 24 hr. A controlled cooling rate of 3K/h was then initiated down to 1273 K when the platinum crucible was removed from the furnace and allowed to cool rapidly to room temperature. To extract the crystals the crucible was immersed in a hot

50% HNO_3 dilute solution. Finally, the crystals were washed in water. In this way, crystals of up to 4 cm^3 were obtained. In order to verify that the M phase was unique some X-ray precession photographs were obtained. These precession photographs show all the crystals to be hexagonal with $a \simeq 5.89$ Å and $c \simeq 23.2$ Å. Taking into account the Laue symmetry, the number of atoms per unit cell and the systematic extinctions observed, hhl, $l = 2n + 1$, only $P\bar{6}2c$, $P6_3mc$, and $P6_3/mmc$ space groups are possible.

For the intensity data collection, a sphere of radius 0.104 mm was mounted on a Philips PW1100 4-circle X-ray diffractometer, using Ag$K\alpha$ radiation. Least-squares refinement of twelve 2θ reflection values, in the range $19° < \theta < 37°$ where complete α_1/α_2 separation occurs, gave the lattice parameters $a = 5.8920(3)$ Å and $c = 23.183(1)$ Å, in good agreement with those determined by Townes (*3*). All reflections from a hemisphere in the interval of 4–28° were measured by the ω-scan technique with a variable scan width $\Delta\theta = (1.40 + 0.20 \tan\theta)$ at the speed of 0.20°/sec. The background was measured at each end of the interval for a time $t = (T_{sc}/2)(I_{bg}/I_{nt})^{1/2}$, where T_{sc} = scan time, I_{bg} = background intensity, I_{nt} = net intensity. A total of 4517 reflections were measured which gave, after averaging according to the $6/mmm$ Laue class, 631 independent reflections. The intensities were converted to structure factors by applying Lorentz polarization and absorption ($\mu R = 0.818$) corrections. Finally, 447 reflections with $|F_{obs}| > 5\sigma(F_{obs})$ were retained. Scattering factor curves for neutral Ba, Fe, and O given by Doyle and Turner (*11*) and anomalous dispersion data of Cromer and Liberman (*12*) were used in the crystal structure refinement.

The structural refinement was carried out with the Enraf-Nonius structure determination package (*13*) and the LINEX least-squares program (adapted from ORFLS) (*14*). An isotropic secondary extinction correction type I (*15*) with a Lorentzian or Gaussian mosaic distribution law has been applied with the LINEX program. The obtained extinction factor value was $G = 0.022(2)$, which corresponds to a mean angular dispersion of the mosaic of 145 sec. Similar final positional and thermal parameters were obtained with the Enraf-Nonius programs taking into consideration reflections such as $\sin\theta/\lambda > 0.35$ and rejecting the 15 strongest reflections, 380 reflections remained in this way. The weights attributed to the reflections during the structure refinement were $w = 1/\sigma^2(F_0)$ where

$$\sigma(F_0) = \sigma(F_0^2)/2F_0, \sigma(F_0^2) = [\sigma^2(I_0) + (0.03I_0^2)]^{1/2}/LP,$$

where $\sigma(I_0)$ is the counting statistics standard deviation.

The structure refinements performed in the noncentrosymmetric $P6_3mc$ and $P\bar{6}2c$ space groups have given nonconclusive results; therefore, the centrosymmetric $P6_3/mmc$ space group has been adopted. The atomic positions reported by Wyckoff (*16*) have been taken.

Two different refinements have been performed, one with the bipyramidal Fe atoms in the $2d$ positions (model 1), and another with these atoms in the $4e$ positions with half occupancy (model 2). In Table I, we report the results obtained for both models with anisotropic and isotropic temperature factors. Atomic position coordinates and temperature factors for the atoms other than Fe2, O1, and O3 do not change, within their standard deviations, with the choice of the model. The obtained R-factors for each case are also indicated in Table I. We note that the best R-factors are those of the model 2 with anisotropic temperature factors ($R = 0.016$, $R_w = 0.021$).

Discussion

The interatomic distances and angles

TABLE I

POSITION AND THERMAL ISOTROPIC AND ANISOTROPIC ($\times 10^5$) PARAMETERS

	Position	x	y	z	β_{11}	β_{22}	β_{33}	β_{12}	β_{13}	β_{23}	B (Å^2)
Ba	2*d*	2/3	1/3	0.25	556(7)	556	26(1)	278	0	0	0.57(1)
Fe1	2*a*	0	0	0	480(18)	480	13(1)	240	0	0	0.41(1)
Fe2	4*e*[a]	0	0	0.25733(4)	420(20)	420	31(2)	210	0	0	0.43(1)
	2*b*[b]	0	0	0.25	365(24)	365	172(3)	182	0	0	1.18(3)
Fe3	4*f*	1/3	2/3	0.02713(2)	417(2)	417	19(1)	208	0	0	0.42(1)
Fe4	4*f*	1/3	2/3	0.19030(2)	473(1)	473	19(1)	236	0	0	0.46(1)
Fe5	12*k*	0.16868	0.33735(7)	−0.10825(1)	455(6)	395(2)	24(1)	197	2	5(2)	0.47(1)
O1	4*e*[a]	0	0	0.15094(13)	472(67)	472	40(4)	236	0	0	0.61(5)
	4*e*[b]						32(4)				0.47(7)
O2	4*f*	1/3	2/3	−0.05454(12)	622(67)	622	13(3)	311	0	0	0.48(5)
O3	6*h*[a]	0.18213	0.36426(47)	0.25	778(50)	389(58)	24(3)	194	0	0	0.66(5)
	6*h*[b]						30(4)				0.82(7)
O4	12*k*	0.15647	0.31294(35)	0.05192(8)	567(3)	487(40)	24(2)	243	3	7(9)	0.56(3)
O5	12*k*	0.50260	1.00520(34)	0.14957(8)	614(32)	638(38)	30(2)	319	23	46(9)	0.68(3)

Note. $T = \exp\left[-\sum_{ij}\beta_{ij}h_ih_j\right] = \exp - B(\sin\theta/\lambda)^2$, by symmetry $\beta_{11} = \beta_{22} = 2\beta_{12}$ and $\beta_{13} = \beta_{23} = 0$ for 2*d*, 2*a*, 4*e*, 4*f* positions; $\beta_{22} = 2\beta_{12}$ and $\beta_{23} = 2\beta_{13}$ for 12*k* position; $\beta_{22} = 2\beta_{12}$ and $\beta_{13} = \beta_{23} = 0$ for 6*h* position.

[a] Model 2: $R = 0.016$, $R_w = 0.021$ for anisotropic temperature factors. $R = 0.022$, $R_w = 0.032$ for isotropic temperature factors.

[b] Model 1: $R = 0.018$, $R_w = 0.025$ for anisotropic temperature factors. $R = 0.042$, $R_w = 0.054$ for isotropic temperature factors.

TABLE II

INTERATOMIC DISTANCES (Å) AND ANGLES (°) IN $BaF_{12}O_{19}$

Ba polyhedron		Fe2 bipyramid	
Ba–O3	× 6 = 2.950(2)	Fe2(I)–O1(IV)	× 1 = 2.128(3) (2.298(3))[b]
Ba–O5	× 6 = 2.868(2)	Fe2(I)–O1(I)	× 1 = 2.468(3) (2.298(3))[b]
⟨Ba–O⟩	2.909	Fe2 –O3	× 3 = 1.867(2) (1.859(2))[b]
O3(I)–O3(II)	× 3 = 2.672(3)	⟨Fe2–O⟩	2.039 (2.035)[b]
O3(I)–O3(III)	× 3 = 3.220(3)	Fe2(I)–Fe2(IV)	× 1 = 0.340(1)
O5(I)–O3(II)	× 6 = 2.900(2)	O1 –O3	× 6 = 2.955(3)
O5(I)–O5(III)	× 12 = 2.850(3)	O3(I)–O3(II)[c]	× 3 = 3.220(3)
O3(I) –Ba(I)–O3(II)	× 3 = 60.1(1)	O1 –O3–O1	× 3 = 102.1(1)
O5(III)–O3(I)–O5(XII)	× 6 = 109.6(1)		
O3(II) –O5(I)–O3(III)	× 6 = 55.9(1)	Fe3 tetrahedron	
O3(I) –Ba(I)–O5(III)	× 12 = 58.6(1)	Fe3–O2	× 1 = 1.894(3)
		Fe3–O4	× 3 = 1.894(2)
Fe1 octahedron		O4(I)–O4(II)	× 3 = 3.126(2)
Fe1–O4	× 6 = 2.000(2)	O4(I)–O2(I)	× 3 = 3.058(3)
O4(VII)–O4(VIII)[a]	× 6 = 2.766(2)		
O4(VII)–O4(XI)	× 6 = 2.889(3)	O2–Fe3–O4	× 3 = 107.7(1)
		O4–O2 –O4	× 3 = 61.5(1)
O4(IX)–Fe1(II)–O4(XII)	× 6 = 87.5(1)		
O4(IX)–Fe1(II)–O4(VIII)	× 6 = 92.5(1)	Fe4 octahedron	
		Fe4–O3	× 3 = 2.073(2)

TABLE II—*Continued*

Fe4–O5	× 3 = 1.969(2)	Important distances and angles	
⟨Fe4–O⟩	2.021	Ba(I) –Fe4(I)	= 3.673(1)
O3(I)–O3(II)[d]	× 3 = 2.672(3)	Ba(I) –Fe2(I)	= 3.406(1)
O3(I)–O5(III)[e]	× 6 = 2.850(3)	Ba(II) –Fe5(I)	= 3.691(1)
O5(I)–O5(III)	× 3 = 2.992(3)	Fe1(I) –Fe3(I)	= 3.460(1)
		Fe1(I) –Fe5(I)[i]	= 3.044(1)
O3(I)–Fe4(I)–O5(I)	× 3 = 166.8(1)	Fe2(I) –Fe4(I)	= 3.740(1)
O3(I)–Fe4(I)–O5(III)	× 6 = 89.6(1)	Fe2(II) –Fe5(III)	= 3.862(1)
O3(I)–Fe4(I)–O3(II)	× 3 = 80.3(1)	Fe2(III)–Fe5(III)	= 3.560(1)
O5(I)–Fe4(I)–O5(III)	× 3 = 98.9(1)	Fe3(I) –Fe5(I)	= 3.561(1)
		Fe3(II) –Fe5(I)	= 3.495(1)
Fe5 octahedron		Fe4(I) –Fe4(IV)[j]	= 2.768(1)
Fe5–O1	× 1 = 1.985(2)	Fe5(I) –Fe5(II)[i]	= 2.911(1)
Fe5–O2	× 1 = 2.092(2)	Fe5(I) –Fe5(III)[i]	= 2.982(1)
Fe5–O4	× 2 = 2.114(3)	Fe2(I) –Fe4(IV)	= 3.612(1)
Fe5–O5	× 2 = 1.932(3)	Fe1(II) –O4(XI)–Fe3(III)	= 126.3(1)
⟨Fe5–O⟩	2.028	Fe1(I) –O4(V) –Fe5(I)	= 95.4(1)
O2(I) –O4(V)	× 2 = 2.949(3)	Fe2(III)–O1(II) –Fe5(III)	= 119.9(1)
O2(I) –O5(V)[f]	× 2 = 2.768(3)	Fe2(I) –O3(III)–Fe4(IV)	= 132.9(1)
O1(II)–O4(V)[f]	× 2 = 2.796(3)	Fe2(I) –O3(III)–Fe4(I)	= 143.3(1)
O1(II)–O5(V)	× 2 = 2.946(3)	Fe3(I) –O2(I) –Fe5(I)	= 126.5(1)
O4(V)–O4(VI)[g]	× 1 = 2.766(3)	Fe3(II) –O4(V) –Fe5(I)	= 121.3(1)
O4(V)–O5(VI)	× 2 = 2.873(3)	Fe4(I) –O3(I) –Fe4(IV)	= 83.8(1)
O5(V)–O5(VI)[h]	× 1 = 2.900(3)	Fe4(II) –O5(VI)–Fe5(I)	= 128.1(1)
		Fe5(I) –O1(II) –Fe5(III)	= 97.3(1)
O2(I) –Fe5(I)–O1(II)	× 1 = 173.3(1)	Fe5(I) –O2(I) –Fe5(III)	= 88.2(1)
O2(I) –Fe5(I)–O4(V)	× 2 = 89.0(1)	Fe5(I) –O5(V) –Fe5(III)	= 97.8(1)
O2(I) –Fe5(I)–O5(V)	× 2 = 86.8(1)	Fe5(I) –O4(V) –Fe5(III)	= 89.7(1)
O1(II)–Fe5(I)–O4(V)	× 2 = 85.9(1)		
O1(II)–Fe5(I)–O5(V)	× 2 = 97.6(1)		

[a] Shared edge with Fe5 octahedra.
[b] Model 1.
[c] Shared edge with Ba polyhedron.
[d] Shared face with Fe4 octahedra and edge with Ba polyhedron.
[e] Shared face with Ba polyhedron.
[f] Shared edge with Fe5 octahedron.
[g] Shared edge with Fe1 octahedron.
[h] Shared edge with Ba polyhedron.
[i] Octahedra with a shared edge.
[j] Octahedra with a shared face.

with their standard deviations for models 1 and 2 are given in Table II. These values were calculated by the BONDLA program of the X-RAY system (*17*). Roman numbers correspond to the equivalent position apparition order in the International Tables for X-Ray Cristallography (*18*). In Table III we report the thermal parameters obtained for models 1 and 2. The coordination polyhedra and the way they link together are shown in Fig. 2. In order to know the way in which the local electric neutrality is accomplished, we have calculated the effective valency of the different ions throughout the structure, taking into account the empirical bond-length to bond-strength relation proposed by Brown and Kun Wu (*19*): $S_{ij} = (D_{ij}/D_1)^{-N}$ where D_1 and N are constants depending on the different cations, S_{ij} is the bond strength and D_{ij} is the inter-

TABLE III
THERMAL ELLIPSOID DATA

Atom	Symmetry	rms (Å)	Angles (°) with the hexagonal axes		
			a	*b*	*c*
Ba	$\bar{6}m2$	0.09	Isotropic		
Fe1	$\bar{3}m$	0.08[a]	0	0	90
		0.06	90	90	0
Fe2	$3m$,[b] $\bar{6}m2$[c]	0.09,[b] 0.22[c]	90	90	0
		0.08,[a] 0.07[a]	0	0	90
Fe3	$3m$	0.07	Isotropic		
Fe4	$3m$	0.08[a]	0	0	90
		0.07	90	90	0
		0.08	90	77	15
Fe5	m	0.08	0	120	90
		0.07	90	33	105
O1	$3m$	0.10	90	90	0
		0.08[a]	0	0	90
O2	$3m$	0.09[a]	0	0	90
		0.06	90	90	0
		0.11	0	120	90
O3	mm	0.08	90	90	0
		0.07	90	30	90
		0.09	0	120	90
O4	m	0.09	90	55	41
		0.08	90	49	131
		0.11	90	51	47
O5	m	0.09	0	120	90
		0.07	90	53	137

[a] Circular section $\perp_z$ due to symmetry.
[b] Model 2.
[c] Model 1.

atomic distance. In this way, the effective valencies for the cations and anions are, respectively, $V_c = \sum_{j=1}^{n} S_{ij}$ and $V_a = \sum_{i=1}^{m} S_{ij}$. The results of these calculations for model 2, with the standard deviations, are reported in Table IV.

R-Block Polyhedra

The R-block, with mirror symmetry at z = 1/4, contains two oxygen layers surrounding the BaO_3 layer, and the Fe2 and Fe4 cations (Fig. 3). The Fe5 octahedra, shared with the neighboring S-blocks, are the limits of the block.

The Ba site has 12-fold coordination with two sets of Ba–O distances: six longer bonds forming an irregular hexagon in the mirror plane (d = 2.950 Å) and six shorter distances with the oxygen in the neighboring layers (d = 2.868 Å), leading to a slightly axially compressed polyhedron. The mean Ba–O distance (d = 2.909 Å) is somewhat shorter than what could be expected from Ba^{2+} effective ionic radius r^{XII} (Ba^{2+}) = 1.60 Å (*20*), consequently the calculated valency is about 16% greater than the theoretical one. Thermal vibration of Ba cation is normal and isotropic.

Beside Ba polyhedron, Fe4 cations form a (Fe_2O_9) group of two octahedra sharing a face in the mirror plane at z = 1/4. In addition, each octahedron shares three faces with different Ba polyhedra. In this configuration the Fe^{3+}–Fe^{3+} electrostatic repulsion separates the cations from each other and the octahedron becomes distorted, with three O3–O3 shorter distances (shared

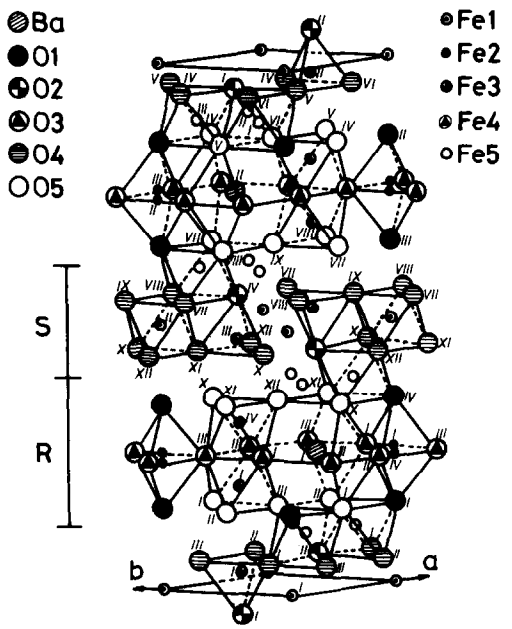

FIG. 2. Coordination polyhedra of cations in Ba $Fe_{12}O_{19}$.

TABLE IV

BOND STRENGTHS AND EFFECTIVE IONIC VALENCIES

$S_{ij} = S_{ji}$	O1	O2	O3	O4	O5	Effective valency
Ba			0.174(×6) (×2)		0.211(×6) (×1)	2.31(1)
Fe1				0.515(×6) (×1)		3.09(2)
Fe2	0.362(×1) (×1/2) 0.155(×1) (×1/2)		0.762(×3) (×1)			2.80(2)
Fe3		0.702(×1) (×1)		0.702(×3) (×1)		2.81(2)
Fe4			0.420(×3) (×2)		0.563(×3) (×1)	2.95(2)
Fe5	0.537(×1) (×3)	0.398(×1) (×3)		0.375(×2) (×2)	0.627(×2) (×2)	2.94(2)
Effective valency	1.87(1)	1.90(2)	1.95(1)	1.97(2)	2.03(2)	

face, d = 2.672 Å) and three O5–O5 longer distances (d = 2.992 Å).

Finally, the R-block contains the Fe2 trigonal bipyramid, a not very common coordination in ferric oxides. This trigonal bipyramid can be regarded as two tetrahedra sharing a face in the mirror plane. These tetrahedra are axially compressed with O3–O3 distances (d = 3.220 Å) much larger than the O3–O1 ones (d = 2.953 Å). These enhanced O3–O3 distances match the correspondingly reduced O3–O3 distances in the shared face of the neighboring Fe4 octahedra, leading to the irregular hexagon surrounding Ba cation in the z = 1/4 mirror plane.

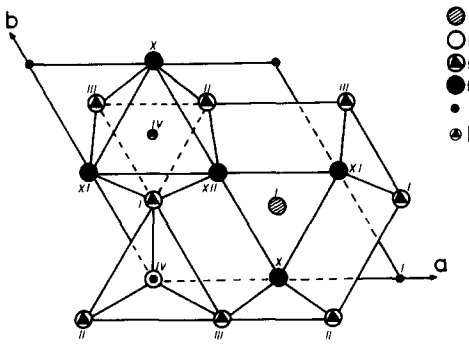

FIG. 3. R-Block polyhedra projected in the Z = 0.25 mirror plane.

It is our purpose to discuss in this paper the consistency of our X-ray data and of previous Mössbauer spectroscopy results (*4–6*) with the three different possibilities for the location and the dynamic characteristics of the bipyramidal Fe2 cations. The X-ray data can help us in the discussion of this problem by means of the study of (i) R-factors and residuals in the Fourier-difference synthesis, (ii) thermal relaxation of surrounding oxygen, and (iii) interatomic distances.

The important difference between R-factors obtained by least-squares refinements of model 1 (R_w = 0.025) and model 2 (R_w = 0.021) gives a high level of statistical significance to the new z parameter introduced for the Fe2 atoms as shown by the Hamilton test (*21*). This result enables us to rule out model 1: Fe2 atom has not a rms thermal amplitude of 0.22 Å along c-axis within a single harmonic potential. This conclu-

sion is confirmed by the appearance, around Fe2 position, of several strong peaks in the Fourier-difference synthesis performed after the least-squares refinement of model 1 (Table V).

At this point, it is clear that only the disordered configurations corresponding to model 2 must be considered. As has been said before, two different possibilities exist for the disorder characteristics of Fe2 atom: a static disorder (model 2a) and a dynamic disorder (model 2b).

It is well known that experiments on elastic scattering of radiation (photons or neutrons) do not furnish any information about the temporal behavior of the atoms: the same atomic positions and thermal parameters would be obtained for a single atom presenting a dynamic or a static disorder, after a crystal structure refinement based on the diffracted Bragg intensities. Nevertheless, we must bear in mind that the consequences of the atomic disorder on its environment may really differ in the two cases. The Mössbauer effect, instead, can give valuable information about the temporal behavior of the atoms. The phase incoherence of photons emitted or absorbed by diffusing Mössbauer nuclei produce a broadened quasielastic resonant component in the Mössbauer spectra (*22, 23*) from which a great variety of dynamic behaviors can be studied (*24–27*). When the inverse of the atom jumping frequency is comparable to the characteristic Mössbauer time ($\tau \sim 10^{-8}$ sec for ^{57}Fe), the quasielastic component is made evident in the Mössbauer spectra and when the jumping frequency is greater than the inverse of the Mössbauer time, the quasielastic component is smeared out in the background resulting only in a reduced effective recoil-free fraction. Therefore, we interpret the low *f*-factors of the bipyramidal ^{57}Fe nuclei observed by Rensen and van Wieringen (*4*) and Mamalui *et al.* (*5*), at high temperatures, as being due to a dynamical disorder configuration (model 2b). The nonobservance of a line broadening in the Mössbauer spectra obtained by Mamalui *et al.* (*5*) and Kreber *et al.* (*6*) at temperatures close to $T = 80$ K may be due to the strong overlap of the bipyramidal subspectra with the remaining sublattices subspectra.

Recapitulating, we can say that only the consideration of both X-ray and Mössbauer spectroscopy results, enables us to conclude that model 1 and model 2a must be disregarded: X-ray results allow us to distinguish between model 1 and model 2, and Mössbauer spectroscopy allows us to disregard model 2a.

Now we will discuss the consistency of the remaining model 2b with the observed thermal, Fourier-map, and structural features.

Thermal ellipsoid parameters of atoms belonging to Fe2 and Ba polyhedra can be observed in Fig. 4 and Table III. We note that O1 ion has its largest vibration along the hexagonal *c*-axis (rms 0.11 Å) whereas O3 anion has its strongest vibration along the *a*-axis (rms 0.11 Å), perpendicular to the mirror plane containing the Fe2–O3 and the Fe4–O3 strong bonds. The fact that O1 ions have a large thermal motion along the

TABLE V

FOURIER-DIFFERENCE PEAKS AROUND Fe2 ATOM AFTER MODEL 1 AND MODEL 2 REFINEMENTS

Model 1[a]		Model 2[b]	
Z[c] (Å)	Electronic density (e^-/Å^3)	Z (Å)	Electronic density (e^-/Å^3)
2.71	+0.48	2.71	+0.42
2.08	−0.78	2.00	−0.59
1.04	+1.07	0.00	+0.28
0.70	−1.92		
0.35	+0.93		

[a] $R = 0.018$; $R_w = 0.025$.
[b] $R = 0.016$; $R_w = 0.021$.
[c] Distance from the BaO_3 mirror plane; $Z(O1) = 2.298$ Å.

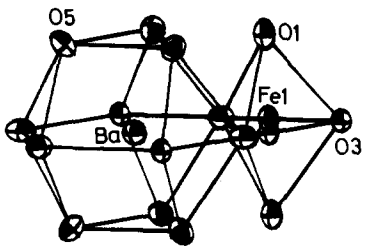

FIG. 4. Thermal ellipsoids in Ba and Fe2 polyhedra (model 2).

trigonal axis of the bipyramid is consistent with the diffusion motion of Fe2 atom along this axis. We remark that the same result would be obtained if model 1 (thermal vibration) or model 2a (mean static displacement) were right. With regard to O3 atoms, their thermal characteristics must be discussed together with the observed interatomic distances. A close relationship is expected to exist between equilibrium position and thermal parameters of O3 ion and the jumping frequency of the neighboring Fe2 atoms. If the jumping frequency were low, the O3 equilibrium positions would be near those expected for a static disorder configuration (model 2a) and if the jumping frequency were high the equilibrium positions would be those expected for the model 1 configuration (Fe2 centered in the bipyramid). In the first case, a large thermal relaxation would exist, while in the second case it would be smaller.

As we have said above, the two unequivalent O3–O3 distances in the BaO_3 mirror plane are very different (3.220 and 2.672 Å). Additional evidence of the fact that these O3–O3 distances are very unusual can be obtained from their comparison with those found in other structures with equivalent local configurations. For example, in the T-block of the hexagonal ferrites (*2*) an equivalent structural configuration does exist, with the unique difference of the bipyramidal site which has been converted to a tetrahedral one. The observed oxygen distances are in this case (*28*): d(O3–O3) = 2.737 Å (2.672 Å in R-block) for the common face of the Fe_2O_9 group and d(O3–O3) = 3.139 Å (3.220 Å in R-block) for the base of the tetrahedron (bipyramid). Therefore, it can be concluded that some additional distorting factors exist in the R-block of the $BaFe_{12}O_{19}$ structure. In this block the O3 atoms of the bipyramid base must move away in order to make the minimum opening of the Fe2 passageway (1.895 Å) compatible with the Fe^{3+} ionic radius. For example, the Fe^{3+}–O distance in YIG tetrahedral sites is 1.865 Å (*29*). When the O3 atoms are located at these new equilibrium positions they vibrate along the weaker bond with a normal amplitude (see Table III).

The validity of the adopted model can also be checked by performing a Fourier-difference synthesis after the crystal structure refinement. By this procedure we found that only around the bipyramidal position did some peaks appear (see Table V). From the comparison of the peaks appearing after the refinement of model 1 and model 2 it is seen that, effectively, model 2 gives a better agreement with the observed electron density. Two peaks, of opposite sign, exist at each side of O1 ion which remain, independently of the chosen model. If we take into account that O1 ion is not placed in a symmetry center, we may interpret these peaks as arising from anharmonicity effects (odd powers of the atomic potential). In this way, the minus sign appearing on the Fe2–O1 bond indicates that a steepest potential does exist at this side.

All these structural and thermal features are consistent with a dynamical disorder of the Fe2 atom (model 2b). Furthermore, they indicate that Fe2 atom oscillates very fast in the double-well potential. As a last remark we suggest that more insight on this disordered configuration could be obtained from a study of the temperature dependence of their structural and thermal fea-

tures as deduced from temperature variable X-ray diffraction data (*30*).

S-Block Polyhedra

The spinel block consists of two oxygen layers stacked in a cubic close-packing fashion with the neighboring layers belonging to the R-block. These two inner layers contain 2 tetrahedral sites (Fe3) and one octahedral site (Fe1) while in the limits of the block 3 octahedral sites (Fe5) are found (Fig. 2). The stacking of this S-block along *c*-axis is the same as the well-known cubic spinel structure along [111] cubic axes. The cationic octahedra share edges among themselves and corners with tetrahedra.

The interatomic distances in the M-structure S-block polyhedra are roughly the same as those in the spinel structure (Table II), except for Fe5 octahedra which are more distorted with point symmetry *m*. The thermal vibrations of cations and anions in this block are normal having orientations such that the strongest bonds are avoided. Fe1 cation has a greater thermal motion within the (001) plane because the interlayer O4–O4 distance is smaller (d = 2.766 Å) than the O4–O4 distance in the layer itself (d = 2.889 Å). The tetrahedral Fe3 cation vibrates isotropically because of its isotropic bond strengths. The strength of the Fe3–O2 bond along z gives to O2 a larger thermal motion in the (001) plane than along the *c*-axis.

Conclusions

Our X-ray single crystal study of $BaFe_{12}O_{19}$ has defined more precisely the structural characteristics proposed by Townes *et al.* (*3*). The dynamical characteristics of the bipyramidal Fe ions have been extensively discussed. From the consideration of our own X-ray results and of the preexisting Mössbauer effect results, the distinction between three a priori structural models have been accomplished. X-Ray diffraction study have enabled us to rule out model 1, in which Fe ions would be found in the center of the trigonal bipyramid with a high thermal motion along the trigonal axis within a single harmonic potential. The existing Mössbauer spectroscopy results allow us to disregard the static disorder configuration (model 2a). In this way, we conclude that the bipyramidal Fe ions stay in a double-well quasiharmonic atomic potential with the two minima at each side of the BaO_3 mirror plane, 0.17 Å away. Within this effective atomic potential the Fe ion presents, at room temperature, a fast diffusional motion between two pseudotetrahedral sites, inducing a supplementary enlargement of the bipyramid base.

Acknowledgments

We are strongly indebted to the referees of the journal for their enlightening suggestions. Dr. E. F. Bertaut, Dr. J. Tejada, and Dr. J. Rodriguez are also acknowledged for many discussions and reading of the manuscript. YEET (Greece), Relations Extérieures (France), and Ministerio de Educación y Ciencia (Spain) are thanked for the financial support of this collaboration.

References

1. V. Aldeskod, *Ark. Kem. Mineral. Geol. Ser. A* **12,** 1 (1938).
2. J. Smit and H. P. J. Wijn, "Ferrites," Philips Tech. Library, Eindhoven (1960).
3. V. D. Townes, J. H. Fang, and A. S. Perrotta, *Z. Kristallogr.* **125,** 437 (1967).
4. J. G. Rensen and J. S. van Wieringen, *Solid State Commun.* **7,** 1139 (1969).
5. Y. A. Mamalui, U. P. Romanov, and K. M. Matsievskii, *Sov. Phys.–Solid State* **21,** 117 (1979).
6. E. Kreber, U. Gonser, A. Trautwein, and F. E. Harris, *J. Phys. Chem. Solids* **36.** 263 (1975).
7. H. B. G. Casimir, J. Smit, U. Enz, J. F. Fast, H. P. J. Wijn, E. W. Gorter, A. J. W. Duyvestein, J. D. Fast, and J. J. de Jongh, *J. Phys. Radium* **20,** 360 (1959).
8. N. Fuchikami, *J. Phys. Soc. Jpn.* **20,** 760 (1965).
9. Y. Xu, G. L. Yang, D. P. Chu, and H. R. Zhai, *J. Magn. Magn. Mater.* **31–34,** 815 (1983).

10. R. J. GAMBINO AND F. W. LEONHARD, *J. Amer. Ceram. Soc.* **44,** 221 (1968).
11. P. A. DOYLE AND P. J. TURNER, *Acta Crystallogr. A* **24,** 390 (1968).
12. D. T. CROMER AND D. LIBERMAN, *J. Chem. Phys.* **53,** 1891 (1970).
13. Structural Determination Package, B. A. Frenz Associates, Inc. College Station Texas 77840, Enraf-Nonius, DELFT, Holland.
14. W. R. BUSING AND H. LEVY, *Acta Crystallogr.* **22,** 457 (1967).
15. P. J. BECKER, *Acta Crystallogr. A* **31,** 1139 (1975).
16. R. W. G. WYCKOFF, "Crystal Structures," Vol. 3, p. 497, Wiley, New York (1965).
17. J. M. STEWART, X-RAY 1963 System, 1971 version, Computer Science Center, University of Maryland College Park, Maryland.
18. "International Tables for X-Ray Crystallography," Vol. I, p. 304, Kynoch Press, Birmingham (1974).
19. I. D. BROWN AND K. KUN WU, *Acta Crystallogr. B* **32,** 1957 (1976).
20. R. D. SHANNON, *Acta Crystallogr. A* **32,** 751 (1976).
21. W. C. HAMILTON, *Acta Crystallogr.* **18,** 502 (1965).
22. K. S. SINGWI AND A. SØLANDER, *Phys. Rev.* **120,** 1093 (1960).
23. M. A. KRIVOGLAZ, *Sov. Phys. JETP (Engl. Transl.)* **13,** 1273 (1961).
24. S. MANTL, W. PETRY, K. SCHROEDER, AND G. VOGL, *Phys. Rev. B* **27,** 5313 (1983).
25. K. H. MAYO, F. PARAK, AND R. L. MÖSSBAUER, Phys. Lett. A **82,** 468 (1981).
26. F. PRÖBST, F. E. WAGNER, AND M. KARGER, *J. Phys. F* **10,** 2081 (1980).
27. F. J. LITTERST, A. LERF, O. NUYKEN, AND H. ALCALÁ, *Hyperfine Interact.* **12,** 317 (1982).
28. W. D. TOWNES AND J. H. FANG, *Z. Kristallogr.* **131,** 196 (1970).
29. F. EULER AND J. A. BRUCE, *Acta Crystallogr. A* **32,** 751 (1976).
30. R. BACHMANN, H. KOHLER, AND H. SCHULZ, "Proceedings, 4th International Conference on Solid State Ionics," Grenoble, France (1983).